Applied Surface Science 504 (2020) 144438

Contents lists available at ScienceDirect

Applied Surface Science

journal homepage: www.elsevier.com/locate/apsusc

Full Length Article

Synthesis and ORR performance of nitrogen-doped ordered microporous carbon by CVD of acetonitrile vapor using silanized zeolite as template

Hongwei Zhao, Lixiang Li*, Yuanyuan Liu, Xin Geng, Haiming Yang, Chengguo Sun, Baigang An*

School of Chemical Engineering, University of Science and Technology Liaoning, Anshan 114051, China
Institute of Energy Materials and Electrochemistry Research, University of Science and Technology Liaoning, Ashan 114051, China

ARTICLE INFO

Keywords:
ORR
CVD of acetonitrile
Nitrogen-doped
Zeolite template
Ordered micropores

ABSTRACT

A simple one-step CVD of acetonitrile vapor was successfully used to prepare nitrogen-doped ordered microporous carbon, where zeolite template was silanized to improve activity of carbon deposition into pore walls of the zeolite, CVD time was used to adjust microstructure and nitrogen containing species. XRD, N_2 adsorption isotherms, SEM, TEM and XPS were used to characterize the composition, microstructure, specific surface area (SSA)/pore distribution and chemical state of nitrogen-doped zeolite-templated carbons (N-ZTCs). Electrochemical tests were carried out to analyze the performance of samples as ORR catalyst. The results show that the N-ZTC as prepared at 750 °C with CVD time of 4 h (N-ZTC-4h) owns ordered micropores, large SSA and abundant nitrogen containing functional groups. As metal free catalyst, N-ZTC-4h exhibits high current density of ORR, good durability and excellent methanol tolerance. Good catalytic ORR performance of N-ZTC-4h is owed to a large quantity of nitrogen containing species with a high ratio of pyridinic-N and quaternary-N owning activity of ORR and the ordered microporous distribution in three-dimensions for mass transport. Easy preparation process and control method of pore structure and nitrogen containing species of N-ZTCs makes it have a big potential in developing nitrogen doped carbon based catalysts of ORR.

1. Introduction

The electrochemical oxygen reduction reaction (ORR) is a crucial step controlling the performance of a variety of energy storage and conversion devices, such as fuel cells and metal-air batteries [1–3]. Due to the sluggish nature of ORR, these devices need employ the catalyst materials, inevitably. Platinum based materials are the most befitting catalysts for ORR in fuel cells, so far [4–6]. However, the high cost, low reserves, poor durability and poor methanol tolerance of Pt-based catalyst have severely hindered the commercialization of these state-of-the-art devices [7–9].

To develop the economical and efficient ORR catalysts, many efforts have been focusing on developing metal-free carbon materials catalysts [10–12]. In this field, heteroatoms doped carbons are attracting more attentions, in particular with nitrogen-doped (N-doped) porous carbons as ORR catalysts [13–15]. Since the nitrogen atoms incorporated into a carbon framework can induce uneven charge density distribution and thereby create active catalytic sites for the ORR. Since Gong et al., reported the high ORR activity of N-doped CNTs in 2009 [16], a variety of N-doped porous carbons, such as carbon nanotubes [17–19], graphene [20,21], carbon xerogel [22–24] and ordered micro/meso-porous carbons [25–28] have been reported as potential alternatives of Pt-based catalysts. These low-cost metal-free catalysts exhibit high ORR activity and durability.

N-doped porous carbons can be prepared by using the following several methods: post-treatment of porous carbons with nitrogen containing gases such as ammonia [29]; pyrolysis of N-containing precursors to deposit N-doped carbon onto porous carbons [30]; direct carbonization of N-containing substances [31]. Nevertheless, it is tough to adjust their pore structure, especially the microporous structure, and to incorporate nitrogen atoms in carbon structure as the same time. It is well-known that the degree of microporosity is a primary factor affecting the properties of porous carbons in many applications. Therefore, it is necessary to control both microporous size and microporous-wall chemical properties to further improve the performance of porous carbons, but such control is a big challenge.

Using zeolite as template to control both microporosity and nitrogen incorporation is a promising approach, by which a variety of zeolite-templated carbons (ZTCs) with ordered micropores and efficient nitrogen doping have been obtained [32–34]. Using the NH_4-impregnated zeolite as a template and the furfuryl alcohol (FA) as a carbon source, Su et al., prepared the N-ZTCs with an ordered micropores, successfully

* Corresponding authors at: School of Chemical Engineering, University of Science and Technology Liaoning, 185 Qianshan zhong Road, Anshan 114051, China.
E-mail addresses: lxli2005@126.com (L. Li), bgan@ustl.edu.cn (B. An).

https://doi.org/10.1016/j.apsusc.2019.144438
Received 5 July 2019; Received in revised form 11 October 2019; Accepted 17 October 2019
Available online 31 October 2019
0169-4332/

[35], whose nitrogen content is ca. 1.84 at% and the specific surface area is up to 3700 $m^2 g^{-1}$. Kyotani's group also developed the two-step method using FA as a primal carbon source and acetonitrile as nitrogen containing source to synthesize N-ZTCs [36]. However, they require an evacuated impregnation of zeolite no less than 24 h for FA filling into micropores and polymerization, and then acetylene CVD was used. These two kinds of methods are time consumed and process complicated. Although Mokaya's and Ryoo's group reported a similar approach of preparation N-doped ZTC through one-step CVD using the mixture gas of acetonitrile and H_2O vapor as precursor [37,38], the specific surface area and ordered microporosity of samples as prepared is significantly lower than the samples prepared by the route of impregnation/polymerization and subsequent CVD. It is probably attributed the low activity of carbon deposition onto the walls of pores.

Herein, through improving the activity of carbon deposition onto the wall of pores by silanizing the zeolite Y template, the N-ZTCs with ordered microporous structure were successfully synthesized by one step CVD of acetonitrile vapor. The pore structure, specific surface area and nitrogen contents of the N-ZTCs were adjusted by controlling CVD time of acetonitrile vapor. The resultant carbon has an ordered microporous structure and large specific surface area. Nitrogen atoms are successfully incorporated in the carbon framework with an amount of 3.0–5.0 at%. The ORR properties of the N-ZTCs were examined and compared. Owing to an efficient nitrogen doping and ordered microporous structure, the N-ZTC exhibits an excellent ORR activity and the better durability and methanol tolerance compared to commercial catalyst of Pt/C. Simple preparation process and good performance of the N-ZTC make it promising catalyst for ORR.

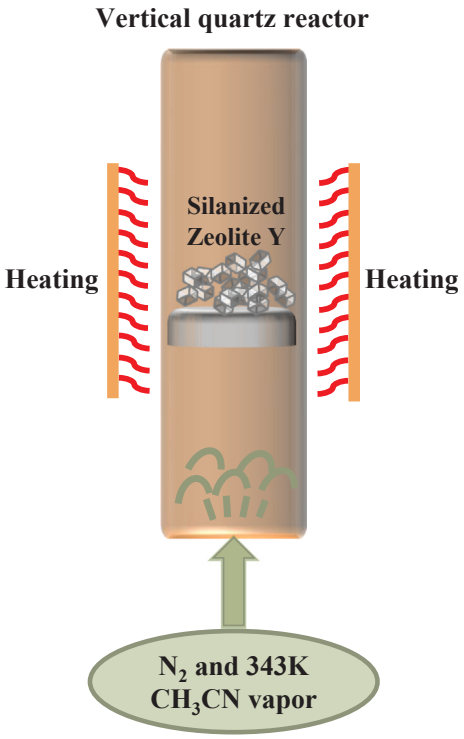

Fig. 1. Schematic illustration of the synthesis device.

2. Experimental

2.1. Chemicals and regents

Hexamethyldisiloxane (HMDS, $C_6H_{18}Si_2O$, 99.0%, Shanghai Aladdin Biochemical Technology Co., Ltd), Isopropyl alcohol (C_3H_8O, A. R. grade, ≥99.0%), Hydrochloric acid (HCl, 5.0 M), Potassium hydroxide (KOH, A. R. grade, ≥99.7%), Acetonitrile (CH_3CN, A. R. grade, ≥99.8%) were purchased from Sinopharm Chemical Reagent Co., Ltd. The zeolite Y (H-form, SiO_2/Al_2O_3 = 5.5, HSZ-320HOA) were obtained from Tosoh (Shanghai) Co., Ltd. Ultrapure C_2H_2, N_2 and O_2 (99.999%) were supplied by the Anshan Angang gas Limited Liability Company.

2.2. Synthesis of N-ZTC

0.8 g zeolite Y, 10.0 mL of hexamethyldisiloxane (HMDS) and 10.0 mL of isopropyl alcohol were added in 15.0 mL 5.0 M HCl and then the solution were stirred with 1 h to mix the components uniformly. Then the solution was kept at the temperature of 80 °C for 1 h. Subsequently, the obtained solid product were filtered and washed several times by isopropyl alcohol and then vacuum dried at 80 °C for 12 h. The obtained solid product was named as silanized zeolite Y. The schematic illustration of device used to synthesize N-ZTCs is shown in Fig. 1. The 0.4 g of silanized zeolite Y in a ceramic boat was placed in a vertical quartz reactor (35 mm in diameter), and then purged by pure nitrogen gas at room temperature for 10 min. The temperature of reactor was heated up to 750 °C under N_2 flow with a heating rate of 5 °C min^{-1}, and then the N_2 flow was switched into an acetonitrile bubbler with 70 °C, which makes the acetonitrile vapor/N_2 flow mixture (0.17 vol% acetonitrile vapor in 100 mL min^{-1} N_2) introduced into the reactor. This CVD of acetonitrile vapor was performed for a given time of 2 h, 4 h and 6 h, respectively, and then the sample was further heat-treated at 900 °C under N_2 flow for 1 h. After that, the temperature of reactor decreased to room temperature under N_2 atmosphere. Finally, the obtained sample was washed by HF/HCl solution at room temperature to liberate carbon part from the zeolite framework. The resultant N-ZTCs was recorded as N-ZTC-X where X represent CVD time of hours. For the sake of comparing, the N-ZTC sample with CVD time of 4 h using zeolite without silanization as template was also prepared.

2.3. Sample characterization

Fourier-transform infrared (FTIR, BRUKER Alpha, KBr pellets) spectra were collected in the range of 400–4000 cm^{-1}. Thermogravimetric analysis (TG, TA SDT-Q600, ceramic crucible, heat rate of 10 °C min^{-1}) curves were collected in the range of room temperature to 900 °C. The morphology and structure of samples were characterized by using scanning electron microscopy (SEM, FEI Apreo, operated at 5 kV), transmission electron microscopy (TEM, FEI Talos F200X, operated at 200 kV), X-ray diffraction device (XRD, Rigaku X'pret Powder, D/MAX-2500X, Cu Kα), Raman spectrometer (HORIBA Xplora Plus, excited by 532 nm laser). The specific surface area (SSA) and pore structure of samples were investigated with an automatic volumetric adsorption/desorption analyzer (Micromeritics, ASAP2020) using N_2 as the adsorbate at −196 °C. The SSA of samples was determined according to the Brunauer Emmett Teller (BET) method within a relative pressure range of 0.05–0.30. The total pore volume (V_{total}) was estimated at P/P_0 = 0.95. The volume of micropore (V_{micro}) and mesopore (V_{meso}) were determined from the DFT cumulative volumes in the pore diameter ranges of $d \leq 2$ nm and 2 nm $< d \leq 50$ nm, respectively. Pore size distribution (PSD) was determined using non-local density functional theory (NLDFT) by assuming the slit-shaped pore geometry. The chemical states of samples were analyzed by X-ray photoelectron spectroscopy (XPS, EscaLabXi+, Al Kα). A binding energy correction was made to account for sample charging based on a C 1s peak at 284.6 eV. The deconvolutions of N 1s spectra were performed using a non-linear least squares fitting program with asymmetric Gaussian function.

2.4. Electrochemical measurements

Electrochemical measurements were performed with an electrochemical analysis system (Reference 3000 workstation and RDE710 Rotating Electrode, Gamry Instruments, USA) with a conventional

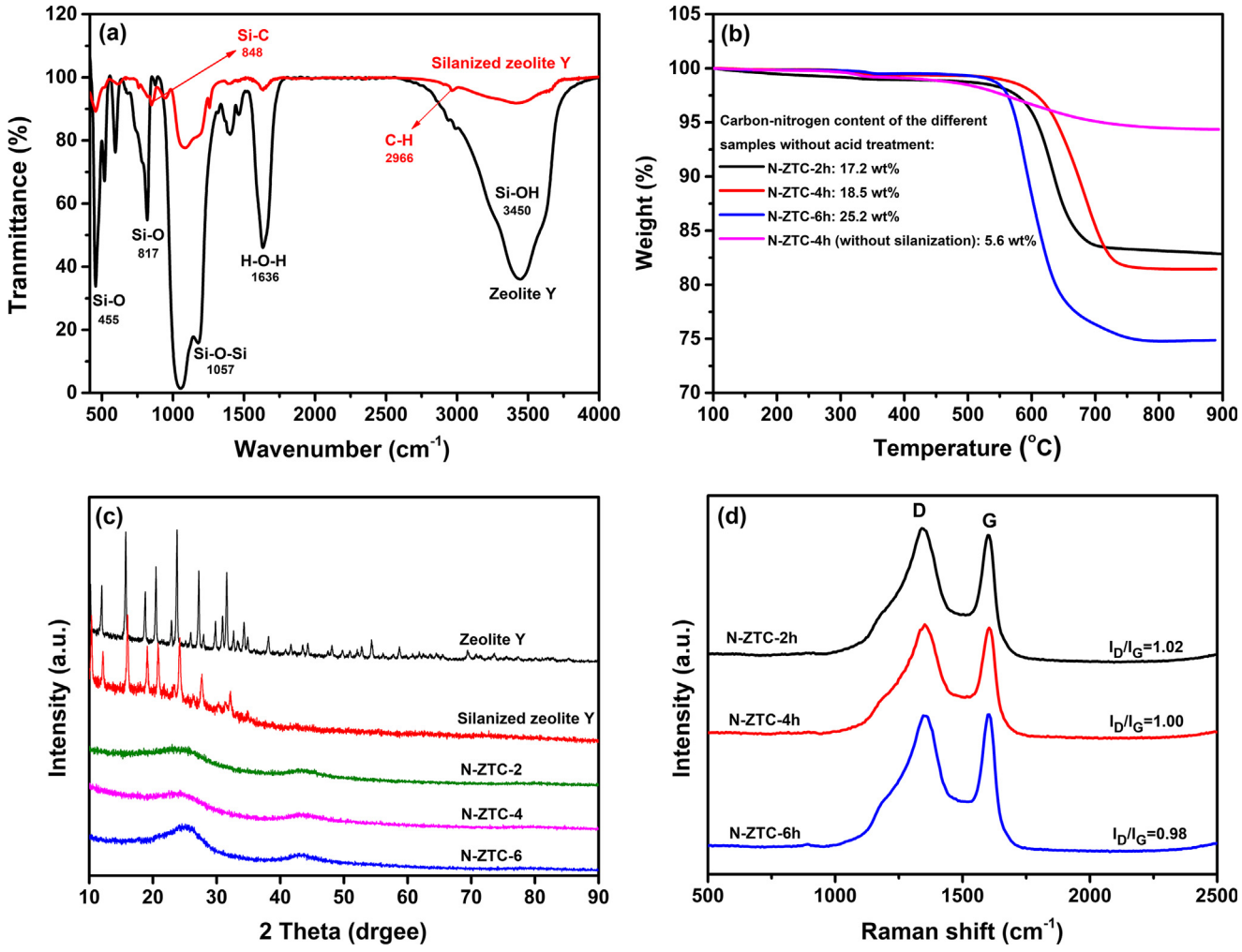

Fig. 2. (a) FTIR spectra of the zeolite Y and silanized zeolite Y, (b) TG curves of N-ZTC samples and N-ZTC-4h (without silanization), (c) XRD patterns and (d) Raman spectra of the samples.

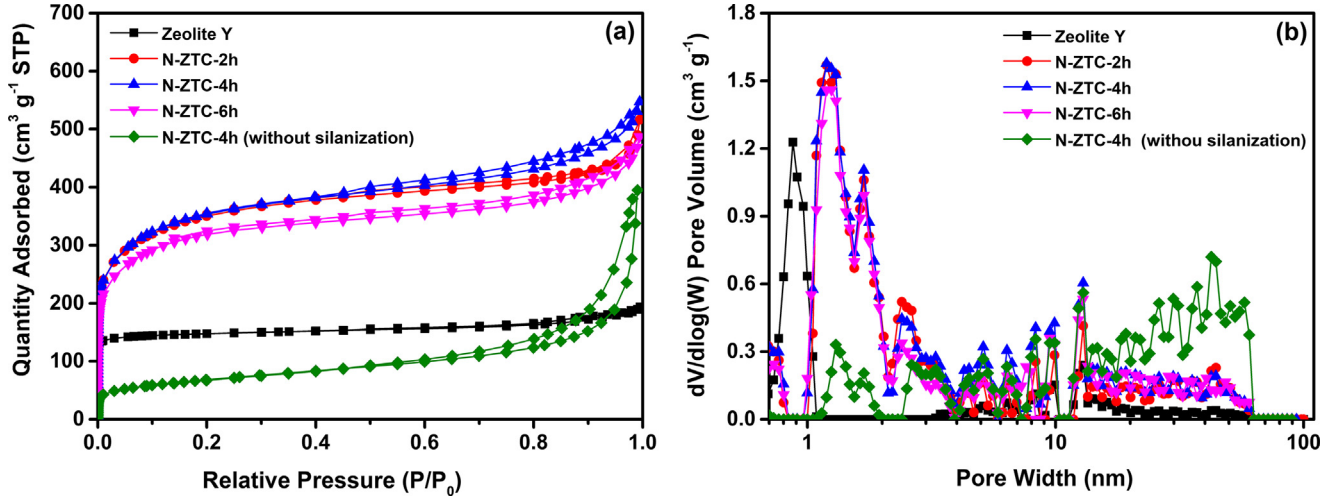

Fig. 3. (a) N_2 adsorption/desorption isotherms of the zeolite Y and N-ZTC samples at −196 °C. (b) DFT PSD of the zeolite Y and N-ZTC samples.

three-electrode cell at room temperature. A glassy carbon electrode (GCE, 6.0 mm in diameter, 0.2826 cm^2 of geometric area) and a rotating disk electrode (RDE, 5.0 mm in diameter, 0.1256 cm^2 of geometric area) coated with the catalyst ink was used as the working electrode. The GCE and RDE were polished by using the slurry of alumina (Al_2O_3, 0.3 and 0.05 μm), then rinsed thoroughly with ethanol and deionized water in an ultrasonic bath to remove any alumina residues. A platinum plate with surface area (1.0 cm^2 of geometric area) was used the counter electrode. The Hg/HgO was chosen as the reference electrode. All the potentials reported in this work were

Table 1
Pore parameters obtained from the N_2 adsorption/desorption isotherms at 77 K for the zeolite Y, N-ZTC samples and N-ZTC-4h-4h without silanization.

Samples	S_{BET} ($m^2 g^{-1}$)	V_{total} ($cm^3 g^{-1}$)	V_{micro} ($cm^3 g^{-1}$)	V_{meso} ($cm^3 g^{-1}$)	V_{micro}/V_{meso}
Zeolite Y	590	0.29	0.18	0.05	0.028
N-ZTC-2h	1284	0.79	0.39	0.20	1.95
N-ZTC-4h	1322	0.84	0.47	0.27	1.77
N-ZTC-6h	1175	0.75	0.40	0.23	1.73
N-ZTC-4h (without silanization)	236	0.53	0.04	0.36	0.11

referenced to the reversible hydrogen electrode (RHE), $E_{RHE} = E_{Hg/HgO} + 0.059\ pH + 0.098$. The electrolyte was 0.1 M KOH solution, which was purged with pure N_2 or O_2 gas for 30 min before electrochemical tests. The catalyst ink was prepared by ultrasonic dispersing 5.0 mg of catalyst powders in 0.5 mL ethanol and 0.45 mL deionized water, into which 50 μL of 5.0 wt% nafion solution (DuPont) was added and the suspension as prepared was ultrasonically dispersed to get the homogenous solution. A quantity of 10 μL of the catalyst ink was pipetted out and dropped on the top surface of GCE. Finally, the GCE coated with the catalyst ink was dried at 25 °C. Cyclic voltammetry (CV) and linear scan voltammetry (LSV) measurement were carried out with a scan rate of 50 mV s^{-1} and 10 mV s^{-1}, respectively. The slopes of their linear-fit lines were used to calculate the number of electrons transfer per oxygen molecule (n) reaction based on the Koutecky-Levich (K-L) equation [12]:

$$\frac{1}{J} = \frac{1}{J_K} + \frac{1}{J_L} = \frac{1}{J_K} + \frac{1}{B\omega^{1/2}}$$

$$B = 0.2nFC_0D_0^{2/3}\upsilon^{-1/6}$$

$$J_K = nFkC_0$$

In the equations, J, J_K and J_L is the measured current density, kinetic current density and limiting diffusion current density, respectively. ω is the angular velocity of disk rotation rates, n is the total electron transfer number of ORR, F (96,485 C mol^{-1}) is the Faraday constant. In the 0.1 M KOH solution, the bulk concentration of oxygen is C_o (1.9×10^{-5} $cm^2 s^{-1}$), and the diffusion coefficient of O_2 is D_o (1.2×10^{-6} mol cm^{-3}).

3. Results and discussion

Since the insert surface of zeolite for carbon deposition, it requires a surface activation treatment to make an efficient CVD of acetonitrile vapor that ensures carbon deposition onto the walls of pores of zeolite template. Surface silanization of zeolite Y using HDMS was tested by FTIR and the results are shown in Fig. 2a. The zeolite Y has several characteristic signals at 3450, 1057, 817 and 455 cm^{-1} are assigned to the bands of Si-OH, Si-O-Si and Si-O, respectively. The signal at 1636 cm^{-1} is attributed to bending mode of adsorbed water (H_2O). After silanization, the signal strength of Si—OH, Si—O, Si—O—Si and adsorbed H_2O for silanized zeolite decreased obviously, respectively, in addition, the C—H band at 2966 cm^{-1} and Si—C band at 848 cm^{-1} can be observed [39–41]. The results indicate that silanization reaction of the surface of zeolite Y with the alcohol hydroxyl after hydrolysis of HMDS. It is well known that hydroxyl and silica groups of template are inactive for carbon deposition. Silanization makes the surface of zeolite matrix coupled with alkyl, which has good activity for carbon deposition. As TG curves shown in Fig. 2b, the carbon deposition content onto the silanized zeolite Y (total amount of carbon and nitrogen) is 17.2 wt % to 25.2 wt% for the N-ZTCs samples prepared by CVD of acetonitrile vapor. However, using the zeolite Y without silanization as template, carbon deposition content is only 5.6 wt% even after 4 h of CVD of acetonitrile vapor.

To get information the composition and the structure of the samples, the X-ray diffraction (XRD) and Raman spectra of the samples were examined. According to the XRD patterns (Fig. 2c), the silanization does not change the structure of zeolite. N-ZTC samples whose two broad diffraction peaks of C (0 0 2) and C (1 0 0) around 2θ of 25.0° and 43.4° become little stronger with increasing CVD time, indicating an enhanced graphitic degree from the sample of N-ZTC-2 h to N-ZTC-6 h. Raman spectroscopy technique has been well demonstrated to characterize the graphitization degree of the carbon materials. As shown in

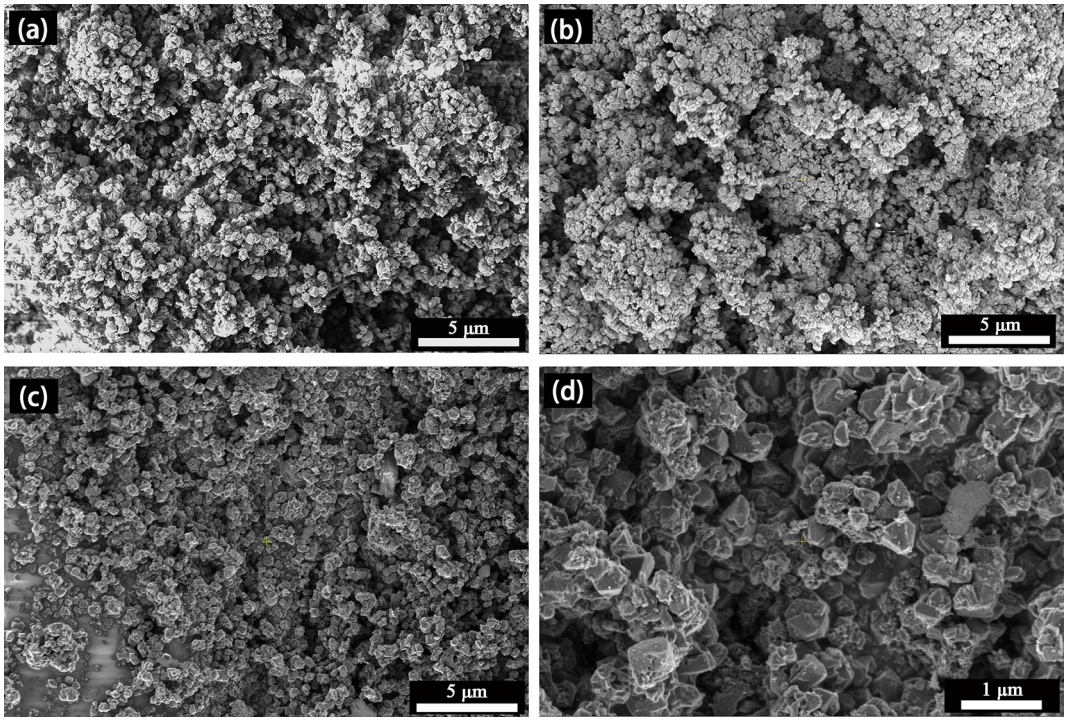

Fig. 4. SEM images of (a) zeolite Y, (b) silanized zeolite Y and (c), (d) N-ZTC-4h.

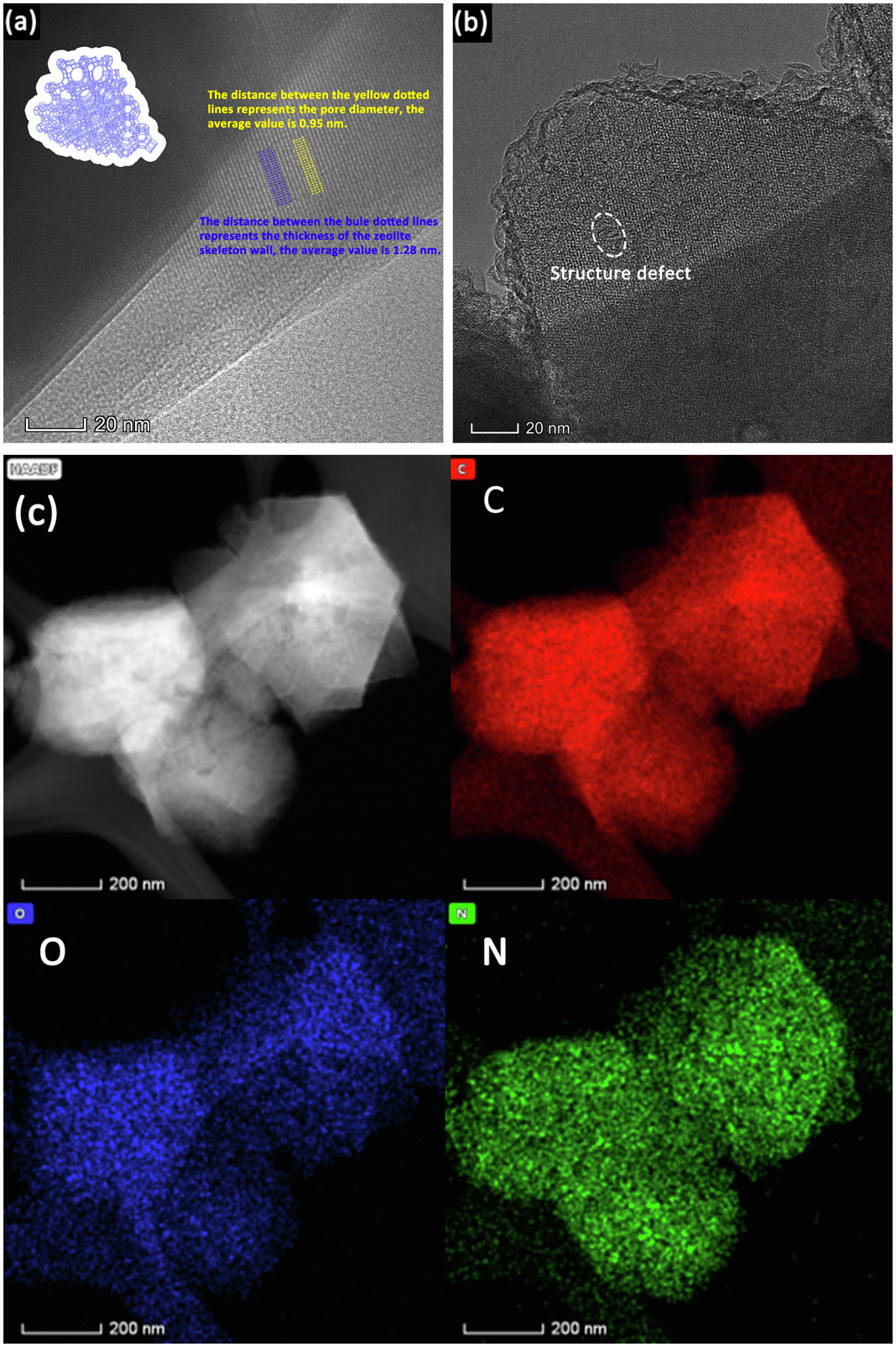

Fig. 5. TEM images of (a) zeolite Y and (b) N-ZTC-4h, (c) HAADF-STEM image of N-ZTC-4h. The corresponding elemental maps of C, O and N within in the (c). The inset of (a) illustrate the zeolite framework structure, and (b) represent the structural defects.

Fig. 2d, the D and G bands at 1350 cm^{-1} and 1590 cm^{-1} can be observed for the N-ZTC samples. The intensity ratio (I_D/I_G) can give us the structural information of materials, and which is inversely proportional to graphitization degree of carbon materials [42]. The I_D/I_G value decreases from N-ZTC-2 h to N-ZTC-6 h in turn, which further confirms that the longer CVD time of acetonitrile vapor result the higher graphitization of N-ZTCs. Although the higher graphitization of N-ZTC benefits to electrons transfer of catalytic reaction, it should be noted that the CVD time can also influences nitrogen doping amount. The amount and types of nitrogen containing groups can impact the activity

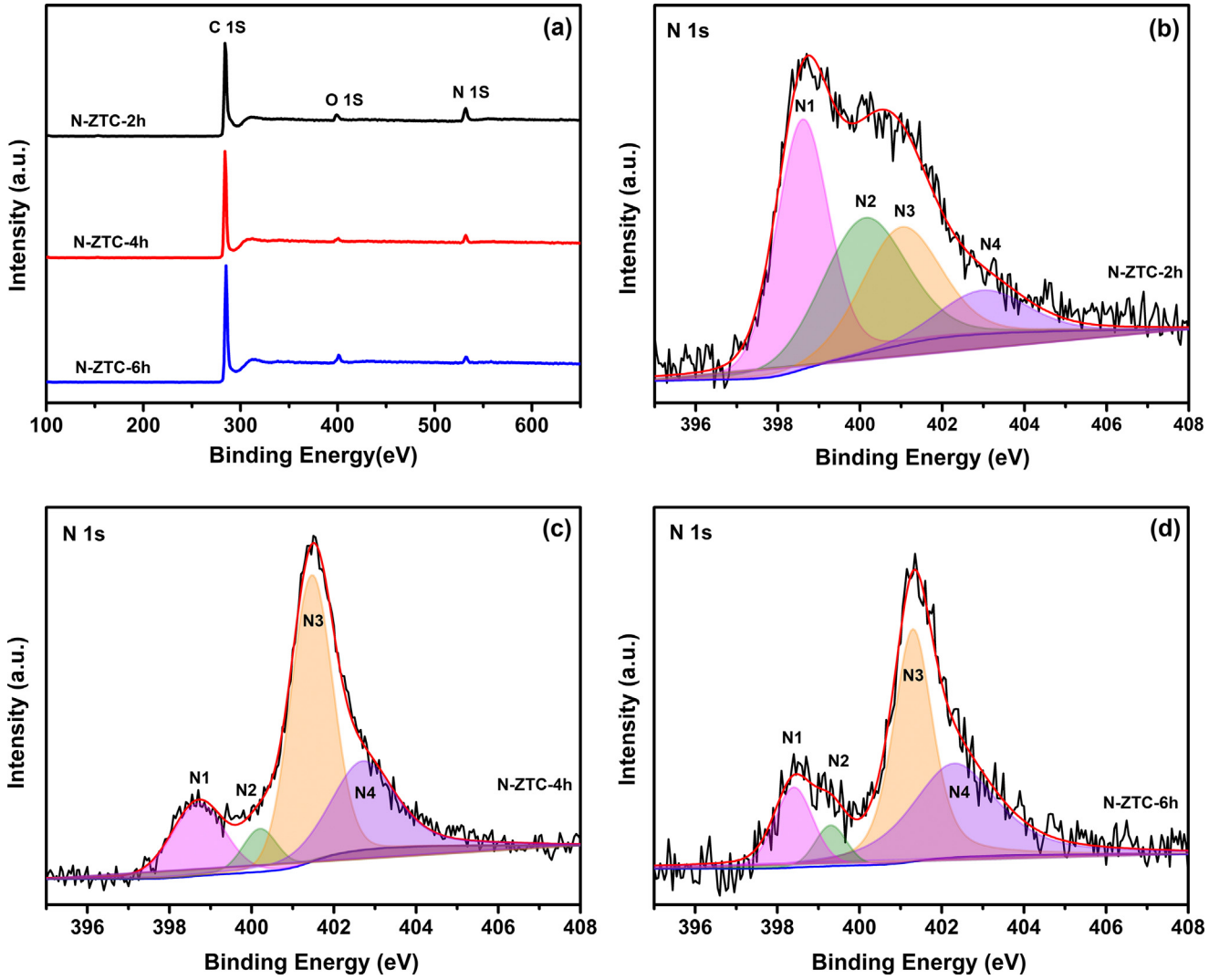

Fig. 6. (a) XPS survey spectra of N-ZTC samples, high-resolution N 1s XPS spectra of (b) N-ZTC-2 h, (c) N-ZTC-4h and (d) N-ZTC-6 h.

Table 2
Surface elements content (at%) and nitrogen-containing functional groups content (at%) obtained by fitting the N 1s level spectra of N-ZTC samples.

Samples	C 1s	O 1s	N 1s	N_1	N_2	N_3	N_4
N-ZTC-2h	88.8	6.1	5.1	1.77	1.55	1.25	0.51
N-ZTC-4h	92.0	2.8	5.2	0.84	0.34	2.60	1.42
N-ZTC-6h	93.3	3.3	3.4	0.45	0.17	1.34	1.44

Note: N_1: Pyridinic-N; N_2: Pyrrolic-N; N_3: Quaternary-N; N_4: Oxide pyridinic-N.

of ORR of N-ZTC catalysts.

The N_2 adsorption/desorption isotherms (Fig. 3a) of N-ZTC samples prepared using silanized zeolite as template all exhibit much higher adsorption capacity than zeolite Y below relative pressure of $P/P_0 = 0.1$, suggesting that the CVD of acetonitrile vapor on silanized zeolite Y results the formation of a large amount of micropores. Compared to zeolite Y template, the isotherms of N-ZTC samples contain a hysteresis loop in the middle relative pressure, which indicates a part of mesopores formed. The high porosity of N-ZTCs originates from the structure of the zeolite Y, where the framework in the nitrogen doped carbon/zeolite composite turns into the local ordered nano-channels of the resulting carbon after etching the inorganic matrix. However, it can be noted that the N-ZTC synthesized using zeolite Y without silanization has much lower adsorption capacity even than zeolite template itself suggesting the collapse of template structure due to low activity of porous walls for carbon deposition. To get further information on porosity of samples, a NLDFT method was applied to determine the pore size distribution (PSD) curves according to the N_2 adsorption/desorption isotherms, which is shown in Fig. 3b. Different from the microporous characteristic of the zeolite Y template (diameter of pore centering around 0.9 nm), the PSD of N-ZTC samples are composed of most micropores located at pore diameter of 1.2 nm and a little part of mesopores. Because the wall thickness of the zeolite Y skeleton is about 1–2 nm [43], the micropores of N-ZTCs should be produced by removal of the template. It is also note that there are a little of ultra micropores with diameter located at 0.5–0.7 nm, which most probably inherits from the original structure of zeolite Y. The walls of micropores were coated with carbon layer due to pyrolysis of acetonitrile vapor resulting pore width decrease. Table 1 gives the parameters of pore and SSA of zeolite Y and N-ZTC samples. The sample prepared without using silanized zeolite as template only has a SSA of 236 $m^2 g^{-1}$, which confirms the structure loss probably owing to the low carbon deposition onto pore walls of unsilanized zeolite. Among the samples, N-ZTC-4h has the highest SSA (1322 $m^2 g^{-1}$) and pore volume (0.84 $cm^3 g^{-1}$) including microporous and mesoporous volume, and thus it could be expected to own a good property as the catalysts of ORR.

The SEM images of zeolite Y before and after silanization and N-ZTC-4h are shown in Fig. 4. All the samples have similarly particular morphology, suggesting that the process of silanization, CVD of

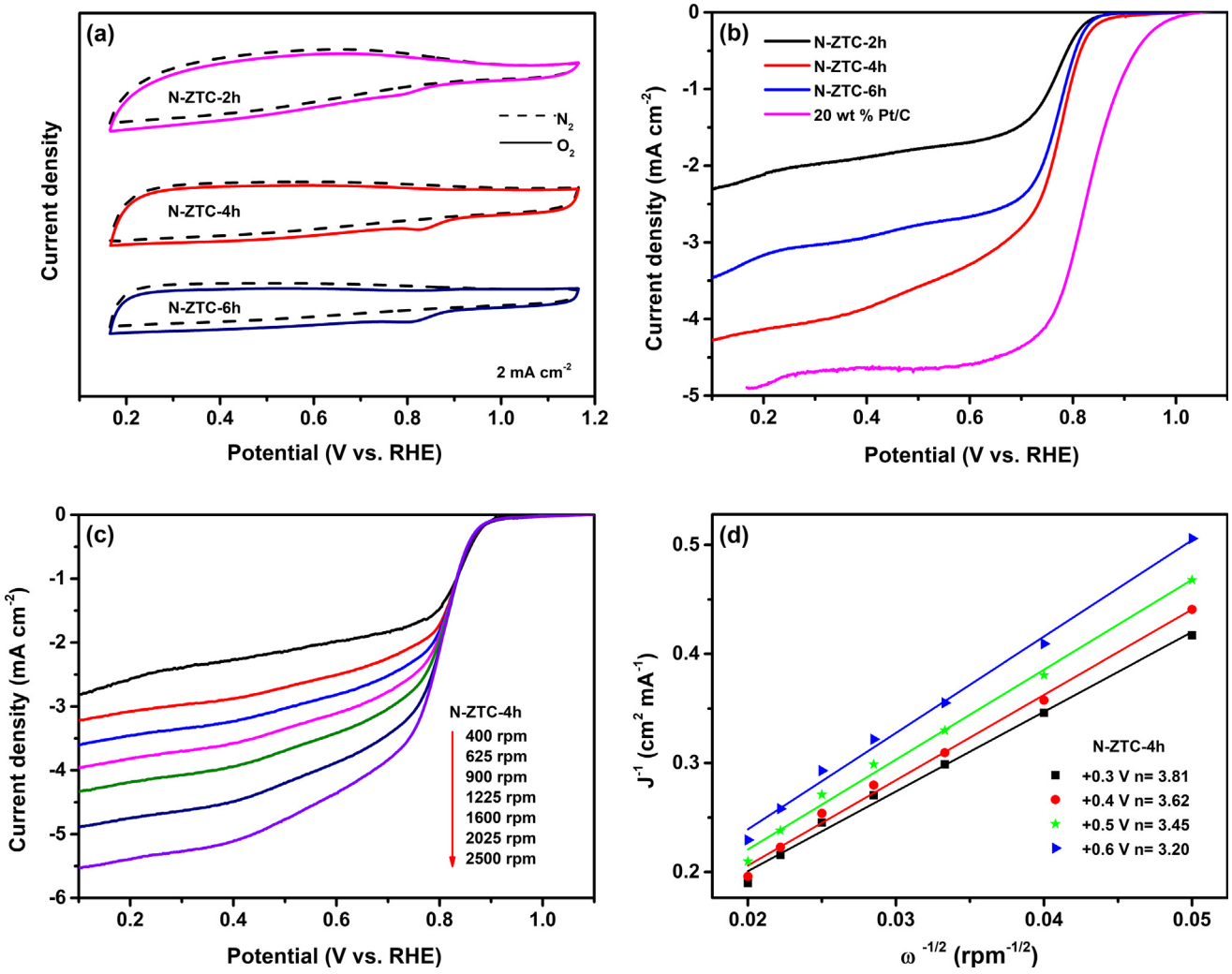

Fig. 7. (a) CV curves of N-ZTC samples in an O_2 (or N_2)-saturated 0.1 M KOH solution at a scanning rate of 50 mV s^{-1}, (b) LSV of N-ZTC samples and 20 wt% Pt/C in an O_2-saturated 0.1 M KOH solution at a scanning rate of 10 mV s^{-1} with rotating rate of 1600 rpm, (c) RDE curves of the N-ZTC-4h in an O_2-saturated 0.1 M KOH solution at a scanning rate of 10 mV s^{-1} with different rotating rates and (d) K-L plots deduced from RDE curves of the N-ZTC-4h.

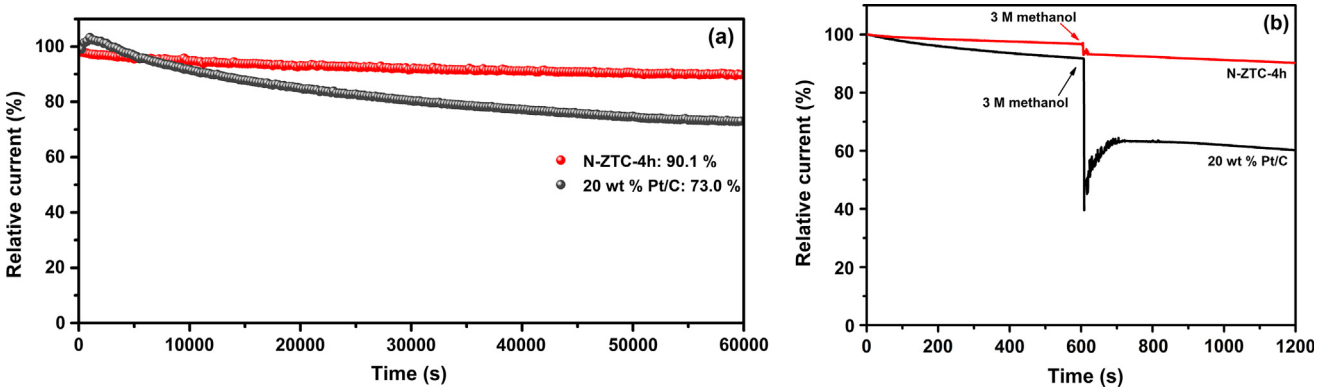

Fig. 8. (a) Chronoamperometric responses of the N-ZTC-4h and commercial catalyst of 20 wt% Pt/C, at + 0.75 V vs. RHE, rotation rate of 900 rpm. (b) The N-ZTC-4h and 20 wt% Pt/C catalysts kept at + 0.75 V vs. RHE when 3 M methanol was added at 600 s, rotation rate of 900 rpm.

acetonitrile vapor and HF/HCl etching does not change the morphology inheriting from zeolite template to the N-ZTC-4h sample, significantly. The HRTEM was further used to observe the microstructure of samples. As shown in Fig. 5a, zeolite Y template owns an ordered pore structure and distribution liking the schematic diagram demonstrated in the inset figure. The ordered arranged bright gray lines and dark gray lines of HRTEM shown in Fig. 5a indicate the ordered distributed pores with very close diameter and the ordered distributed pore walls of zeolite Y template, respectively. According to the statistics of thickness of these bright gray lines and dark bray lines, the average pore diameter and pore wall thickness of zeolite Y template is 0.95 nm and 1.28 nm, respectively. Since N-ZTC-4h is an inverse copy of zeolite Y template, its microstructure inherits the characteristic of the template. The highly ordered distribution of micropores in N-ZTC-4h can be clearly observed

in Fig. 5b, meanwhile some structural defects that disordered pores distributed in a few area of sample can be distinguished by comparing TEM images of zeolite Y template and N-ZTC-4h, which could be caused by nitrogen doping process. Elemental mapping of N-ZTC-4h measured by electronic diffraction spectroscopy (EDS) is shown in Fig. 5c, the results show that the elements of C, O, and N are uniformly distributed in the particles of N-ZTC-4h, suggesting the successful nitrogen doping by acetonitrile vapor CVD. Elemental mapping of N-ZTC-4h measured by electronic diffraction spectroscopy (EDS) is shown in Fig. 5c, the results show that the elements of C, O, and N are uniformly distributed in the particles of N-ZTC-4h, suggesting the successful nitrogen doping by acetonitrile vapor CVD.

X-ray photoelectron spectroscopy (XPS) is a useful tool to study the surface composition of materials. Fig. 6a is the XPS survey spectra of the samples, the peaks around binding energy of 284.5, 398.5 and 532.2 eV are assigned to C 1s, N 1s, and O 1s. Table 2 gives the relative atomic percentage of C, O, and N of N-ZTC samples. The nitrogen content of N-ZTC-4h (5.2 at%) is little higher than the N-ZTC-2 h (5.1 at%), but the increasing CVD of acetonitrile time to 6 h results the lower content of nitrogen (3.4 at%) of N-ZTC-6 h. In addition to nitrogen doping amount, the types of nitrogen containing functional groups have an important impact on ORR property of nitrogen doped carbons. XPS N 1s spectra of N-ZTC samples were (Fig. 6b–d) fitted by four overlapping peaks at 398.6, 400.2, 401.5 and 402.7 eV of binding energy, which can be assigned to the different states of nitrogen atoms of N_1 (pyridinic-N), N_2 (pyrrolic-N), N_3 (quaternary-N), and N_4 (oxide pyridinic-N), respectively [44,45]. The content of nitrogen atoms with different states summarized in Table 2 shows that N-ZTC-4h owns the largest total amount of pyridinic-N and quaternary-N. It have been demonstrated that these two types of doped nitrogen in carbons contribute a good activity toward ORR [46]. Based on the XPS analysis results, the N-ZTC-4h has not only the largest total amount of nitrogen containing species but also the largest ratio of pyridinic-N and quaternary-N benefitting activity of ORR, and thus is expected to own good performance as ORR catalyst [13,47].

The catalytic activity of N-ZTCs toward ORR was evaluated by electrochemical method. Cyclic voltammograms (CV) of samples in O_2 or N_2 gas-saturated 0.1 M KOH solution are shown in Fig. 7a. Although the capacitive behavior of electric double layer due to the porosity and large SSA of N-ZTCs, the ORR peaks can be observed for the samples. The ORR peak potential from N-ZTC-2 h to N-ZTC-6 h is 0.79, 0.84 and 0.82 V (vs. RHE) in turns, N-ZTC-4h exhibits the most positive ORR peak potential indicating its good activity of ORR. To further insight the ORR activity of samples, linear scan voltammetry (LSV) measurements were performed and the results are shown in Fig. 7b. Among the N-ZTC samples, the N-ZTC-4h own the highest limiting current density and relatively positive onset potential for ORR, again demonstrates good activity for ORR. Although, they are still little lower than the commercial catalyst of 20 wt% Pt/C. The ordered microporous characteristic, high SSA combining with a large amount of nitrogen doping and a big ratio of pyridinic-N and quaternary-N in nitrogen containing species of N-ZTC-4h should contribute to its good activity as ORR metal free catalyst. Moreover, according to the LSV of N-ZTC-4h tested with a rotating disk electrode (RDE) at different rotation rates from 400 to 2500 rpm as shown in Fig. 7c, the corresponded K–L plots of J^{-1} versus $\omega^{-1/2}$ was obtained (Fig.Fig. 7d), and then the number of electrons transfer for ORR of catalyst was calculated through K-L equation. The results demonstrates that the electron-transfer number for the N-ZTC-4h catalyst toward ORR was calculated to be between 2 and 4, which indicates that the two-electron and four-electron pathways were simultaneously involved in the oxygen reduction.

Durability and methanol tolerance is still a major problem of Pt based catalysts facing to. The N-ZTC-4h exhibits an excellent durability and the methanol tolerance as shown in Fig. 8. The chronoamperometric measurement at +0.75 V (vs. RHE) shows that the retention ratio of the current density for N-ZTC-4h can achieve to 90.1% after continuous operation for 60000 s, whereas it is only 73.0% for the 20 wt % Pt/C catalyst. The excellent durability of N-ZTC-4h can be attributed to its ordered microporous distribution in three-dimensions for mass transport, stable nitrogen containing species of pyridinic/quaternary-N for ORR catalysis, meanwhile good graphitization degree for electrons transfer. The methanol tolerance of the catalysts was characterized by observing the current stability when some amount of methanol was added into a 0.1 M KOH solution during chronoamperometric measurement. A dramatic decrease of ORR relative current can be found for 20 wt% Pt/C catalyst and the current cannot recover to the previous value before adding methanol. However, there is only a slight change of ORR current before and after adding methanol for N-ZTC-4h electrode.

4. Conclusions

Nitrogen-doped ordered microporous carbon was successfully synthesized by one-step CVD of acetonitrile vapor using the silanized zeolite as template. The optimized samples of N-ZTC-4h with a large SSA of 1322 m^2 g^{-1}, most of ordered micropores, a big quantity of nitrogen containing functional groups of 5.2 at% was obtained by simply adjusting CVD time. As metal free catalyst for ORR, the N-ZTC-4h sample exhibits good performance by evaluating its onset potential, oxygen diffusion limiting current, durability and methanol tolerance as ORR catalyst. Good property of N-ZTC-4h as metal free catalyst could be attributed to its ordered microporous distribution in three-dimensions for mass transport, a large amount of nitrogen containing species owning ORR activity, especially the pyridinic and quaternary nitrogen species. The simple process for preparing N-doped ordered microporous carbon and adjusting its structure makes N-ZTCs promising catalysts for ORR.

Declaration of Competing Interest

The authors declared that there is no conflict of interest.

Acknowledgement

The financial supports from NSFC projects of No. 51672117, 51672118, 51872131 and 21701077, and the Project of Education Department of Liaoning No. 2017LNZD01 are acknowledged.

References

[1] J. Zhu, M. Xiao, P. Song, J. Fu, Z. Jin, L. Ma, J. Ge, C. Liu, Z. Chen, W. Xing, Highly polarized carbon nano-architecture as robust metal-free catalyst for oxygen reduction in polymer electrolyte membrane fuel cells, Nano Energy 49 (2018) 23–30.
[2] G. Wu, K.L. More, C.M. Johnston, P. Zelenay, High-performance electrocatalysts for oxygen reduction derived from polyaniline, iron, and cobalt, Science 332 (2011) 443–447.
[3] T. Sun, J. Wang, C. Qiu, X. Ling, B. Tian, W. Chen, C. Su, B, N codoped and defect-rich nanocarbon material as a metal-free bifunctional electrocatalyst for oxygen reduction and evolution reactions, Adv. Sci. 5 (2018) 1800036.
[4] K. Jiang, D. Zhao, S. Guo, X. Zhang, X. Zhu, J. Guo, G. Lu, X. Huang, Efficient oxygen reduction catalysis by subnanometer Pt alloy nanowires, Sci. Adv. 3 (2017) e1601705.
[5] S. Sui, X. Wang, X. Zhou, Y. Su, S. Riffat, C.J. Liu, A comprehensive review of Pt electrocatalysts for the oxygen reduction reaction: nanostructure, activity, mechanism and carbon support in PEM fuel cells, J. Mater. Chem. A 5 (2017) 1808–1825.
[6] Y.J. Wang, W. Long, L. Wang, R. Yuan, A. Ignaszak, B. Fang, D.P. Wilkinson, Unlocking the door to highly active ORR catalysts for PEMFC applications: polyhedron-engineered Pt-based nanocrystals, Energy Environ. Sci. 11 (2018) 258–275.
[7] Y.J. Wang, N. Zhao, B. Fang, H. Li, X.T. Bi, H. Wang, Carbon-supported Pt-based alloy electrocatalysts for the oxygen reduction reaction in polymer electrolyte membrane fuel cells: particle size, shape, and composition manipulation and their impact to activity, Chem. Rev. 115 (2015) 3433–3467.
[8] L. Zhang, Y. Zhao, M.N. Banis, K. Adair, Z. Song, L. Yang, M. Markiewicz, J. Li, S. Wang, R. Li, S. Ye, X. Sun, Rational design of porous structures via molecular layer deposition as an effective stabilizer for enhancing Pt ORR performance, Nano Energy 60 (2019) 111–118.
[9] H. Yano, M. Watanabe, A. Iiyama, H. Uchida, Particle-size effect of Pt cathode catalysts on durability in fuel cells, Nano Energy 29 (2016) 323–333.

[10] L. Dai, Y. Xue, L. Qu, H.J. Choi, J.B. Baek, Metal-free catalysts for oxygen reduction reaction, Chem. Rev. 115 (2015) 4823–4892.
[11] J. Wang, J. Hao, D. Liu, S. Qin, D. Portehault, Y. Li, Y. Chen, W. Lei, Porous boron carbon nitride nanosheets as efficient metal-free catalysts for the oxygen reduction reaction in both alkaline and acidic solutions, ACS Energy Lett. 2 (2017) 306–312.
[12] Z. Zhou, A. Chen, X. Fan, A. Kong, Y. Shan, Hierarchical porous N-P-coupled carbons as metal-free bifunctional electro-catalysts for oxygen conversion, Appl. Surf. Sci. 464 (2019) 380–387.
[13] P. Yan, J. Liu, S. Yuan, Y. Liu, W. Cen, Y. Chen, The promotion effects of graphitic and pyridinic N combinational doping on graphene for ORR, Appl. Surf. Sci. 445 (2018) 398–403.
[14] Z. Liu, F. Sun, L. Gu, G. Chen, T. Shang, J. Liu, Z. Le, X. Li, H.B. Wu, Y. Lu, Post iron decoration of mesoporous nitrogen-doped carbon spheres for efficient electrochemical oxygen reduction, Adv. Energy Mater. 7 (2017) 1701154.
[15] H. Han, Y. Noh, Y. Kim, W.S. Jung, S. Park, W.B. Kim, An N-doped porous carbon network with a multidirectional structure as a highly efficient metal-free catalyst for the oxygen reduction reaction, Nanoscale 11 (2019) 2423–2433.
[16] K. Gong, F. Du, Z. Xia, M. Durstock, L. Dai, Nitrogen-doped carbon nanotube arrays with high electrocatalytic activity for oxygen reduction, Science 323 (2009) 760.
[17] R. Du, N. Zhang, J. Zhu, Y. Wang, C. Xu, Y. Hu, N. Mao, H. Xu, W. Duan, L. Zhuang, L. Qu, Y. Hou, J. Zhang, Nitrogen-doped carbon nanotube aerogels for high-performance ORR catalysts, Small 11 (2015) 3903–3908.
[18] W. Liu, Q. Ru, S. Zuo, S. Yang, J. Han, C. Yao, Controllable synthesis of nitrogen-doped carbon nanotubes derived from halloysite-templated polyaniline towards nonprecious ORR catalysts, Appl. Surf. Sci. 469 (2019) 269–275.
[19] D.C. Higgins, M.A. Hoque, F. Hassan, J.Y. Choi, B. Kim, Z. Chen, Oxygen reduction on graphene-carbon nanotube composites doped sequentially with nitrogen and sulfur, ACS Catal. 4 (2014) 2734–2740.
[20] T. Xing, Y. Zheng, L.H. Li, B.C. Cowie, D. Gunzelmann, S.Z. Qiao, S. Huang, Y. Chen, Observation of active sites for oxygen reduction reaction on nitrogen-doped multilayer graphene, ACS Nano 8 (2014) 6856–6862.
[21] M. Rahsepar, M.R. Nobakht, H. Kim, M. Pakshir, Facile enhancement of the active catalytic sites of N-doped graphene as a high performance metal-free electrocatalyst for oxygen reduction reaction, Appl. Surf. Sci. 447 (2018) 182–190.
[22] H. Jin, H. Zhang, H. Zhong, J. Zhang, Nitrogen-doped carbon xerogel: a novel carbon-based electrocatalyst for oxygen reduction reaction in proton exchange membrane (PEM) fuel cells, Energy Environ. Sci. 4 (2011) 3389.
[23] H. Jin, J. Li, F. Chen, L. Gao, H. Zhang, D. Liu, Q. Liu, Nitrogen-doped carbon xerogels as novel cathode electrocatalysts for oxygen reduction reaction in direct borohydride fuel cells, Electrochim. Acta 222 (2016) 438–445.
[24] S. Liu, H. Zhang, Z. Xu, H. Zhong, H. Jin, Nitrogen-doped carbon xerogel as high active oxygen reduction catalyst for direct methanol alkaline fuel cell, Int. J. Hydrog. Energy 37 (2012) 19065–19072.
[25] A. Castro-Muñiz, H. Nishihara, T. Hirota, M. Ohwada, L.X. Li, T. Tsuda, S. Kuwabata, J. Maruyama, T. Kyotani, Boron and nitrogen co-doped ordered microporous carbons with high surface areas, Chem. Commun. 53 (2017) 13348–13351.
[26] X. Li, H. Wang, J.T. Robinson, H. Sanchez, G. Diankov, H. Dai, Simultaneous nitrogen doping and reduction of graphene oxide, J. Am. Chem. Soc. 131 (2009) 15939–15944.
[27] H. Nishihara, T. Kyotani, Zeolite-templated carbons-three-dimensional microporous graphene frameworks, Chem. Commun. 54 (2018) 5648–5673.
[28] J. Xu, Y. Zhao, C. Shen, L. Guan, Sulfur- and nitrogen-doped, ferrocene-derived mesoporous carbons with efficient electrochemical reduction of oxygen, ACS Appl. Mater. Interfaces 5 (2013) 12594–12601.
[29] J. Wang, R. Ma, Y. Zhou, Q. Liu, A facile nanocasting strategy to nitrogen-doped porous carbon monolith by treatment with ammonia for efficient oxygen reduction, J. Mater. Chem. A 3 (2015) 12836–12844.
[30] B.G. An, S.F. Xu, L.X. Li, J. Tao, F. Huang, X. Geng, Carbon nanotubes coated with a nitrogen-doped carbon layer and its enhanced electrochemical capacitance, J. Mater. Chem. A 1 (2013) 7222–7228.
[31] L. Hou, L. Lian, D. Li, G. Pang, J. Li, X. Zhang, S. Xiong, C. Yuan, Mesoporous N-containing carbon nanosheets towards high-performance electrochemical capacitors, Carbon 64 (2013) 141–149.
[32] C. Xue, H. Zhu, T. Xu, E. Wang, B. Xiao, X. Liu, X. Hao, G. Guan, Zeolite cage-lock strategy for in situ synthesis of highly nitrogen-doped porous carbon for selective adsorption of carbon dioxide gas, RSC Adv. 7 (2017) 24195–24203.
[33] H. Itoi, H. Nishihara, T. Kyotani, Effect of heteroatoms in ordered microporous carbons on their electrochemical capacitance, Langmuir 32 (2016) 11997–12004.
[34] R.J. Konwar, M. De, Effects of synthesis parameters on zeolite templated carbon for hydrogen storage application, Microporous Mesoporous Mater. 175 (2013) 16–24.
[35] F. Su, X.S. Zhao, L. Lv, Z. Zhou, Synthesis and characterization of microporous carbons templated by ammonium-form zeolite Y, Carbon 42 (2004) 2821–2831.
[36] P.X. Hou, H. Orikasa, T. Yamazaki, K. Matsuoka, A. Tomita, N. Setoyama, Y. Fukushima, T. Kyotani, Synthesis of nitrogen-containing microporous carbon with a highly ordered structure and effect of nitrogen doping on H_2O adsorption, Chem. Mater. 17 (2005) 5187–5193.
[37] Z. Yang, Y. Xia, R. Mokaya, Enhanced hydrogen storage capacity of high surface area zeolite-like carbon materials, J. Am. Chem. Soc. 129 (2007) 1673–1679.
[38] Y. Kwon, K. Kim, R. Ryoo, N-doped zeolite-templated carbon as a metal-free electrocatalyst for oxygen reduction, RSC Adv. 6 (2016) 43091–43097.
[39] T. Kaneko, D. Nemoto, A. Horiguchi, N. Miyakawa, FTIR analysis of a-SiC: H films grown by plasma enhanced CVD, J. Cryst. Growth 275 (2005) e1097–e1101.
[40] Y. Fang, P.S.J. Lakey, S. Riahi, A.T. McDonald, M. Shrestha, D.J. Tobias, M. Shiraiwa, V.H. Grassian, A molecular picture of surface interactions of organic compounds on prevalent indoor surfaces: limonene adsorption on SiO_2, Chem. Sci. 10 (2019) 2906–2914.
[41] J. Percino, J.A. Pacheco, G. Soriano-Moro, M. Cerón, M.E. Castro, V.M. Chapela, J. Bonilla-Cruz, T.E. Lara-Ceniceros, M. Flores-Guerrero, E. Saldivar-Guerra, Synthesis, characterization and theoretical calculations of model compounds of silanols catalyzed by TEMPO to elucidate the presence of Si-O-Si and Si-O-N bonds, RSC Adv. 5 (2015) 79829–79844.
[42] Y. Jiang, Y. Lu, X. Lv, D. Han, Q. Zhang, L. Niu, W. Chen, Enhanced catalytic performance of Pt-free iron phthalocyanine by graphene support for efficient oxygen reduction reaction, ACS Catal. 3 (2013) 1263–1271.
[43] C.O. Ania, V. Khomenko, E. Raymundo-Piñero, J.B. Parra, F. Béguin, The large electrochemical capacitance of microporous doped carbon obtained by using a zeolite template, Adv. Funct. Mater. 17 (2007) 1828–1836.
[44] S. Ratso, N. Ranjbar Sahraie, M.T. Sougrati, M. Käärik, M. Kook, R. Saar, P. Paiste, Q. Jia, J. Leis, S. Mukerjee, F. Jaouen, K. Tammeveski, Synthesis of highly-active Fe-N-C catalysts for PEMFC with carbide-derived carbons, J. Mater. Chem. A 6 (2018) 14663–14674.
[45] J.C. Li, S.Y. Zhao, P.X. Hou, R.P. Fang, C. Liu, J. Liang, J. Luan, X.Y. Shan, H.M. Cheng, A nitrogen-doped mesoporous carbon containing an embedded network of carbon nanotubes as a highly efficient catalyst for the oxygen reduction reaction, Nanoscale 7 (2015) 19201–19206.
[46] S.W. Han, J. Bang, S.H. Ko, R. Ryoo, Variation of nitrogen species in zeolite-templated carbon by low-temperature carbonization of pyrrole and the effect on oxygen reduction activity, J. Mater. Chem. A 7 (2019) 8353–8360.
[47] Z.L. Wang, D. Xu, J.J. Xu, X.B. Zhang, Oxygen electrocatalysts in metal-air batteries: from aqueous to nonaqueous electrolytes, Chem. Soc. Rev. 43 (2014) 7746–7786.